New Self-Healing Dielectric for High-Reliability, High-Performance PCB-Embedding Materials for Power Electronics Applications

Baptiste Arati, Vincent Bley, Pierre-Yves Pichon, Gilbert Teyssedre

Cite as: B. Arati, V. Bley, P.-Y. Pichon, G. Teyssedre, "*New self-healing dielectric for high-reliability, high-performance PCB-embedding materials for power electronics applications*," IEEE Access 11, pp. 133967-133978, 2023. *DOI: 10.1109/ACCESS.2023.3334632*

New self-healing dielectric for high-reliability, high-performance PCB-embedding materials for power electronics applications

B. Arati[1,2], V. Bley[1], P-Y. Pichon.[2], G. Teyssedre[1]
[1]LAPLACE, University of Toulouse; CNRS-UPS, INPT; Toulouse, France
[2]Mitsubishi Electric R&D Centre Europe, Rennes, France

ABSTRACT Printed Circuit Board (PCB)-embedded power electronics packages are anticipated as the next major packaging trend to support efficient and reliable electrical energy conversions. With many core aspects of the package being modified, the dielectric is now required to ensure new functions while still assuming its original electrical insulation function. With the expected increase of operational voltages that come with wide bandgap semiconductor components, high-reliability dielectric packaging materials are required. Given the recent breakthrough in polymeric science, self-healing materials based on Covalent Adaptable Networks (CANs) can be applied to highly stressed systems such as integrated power modules, with the aim to improve the reliability of the package. This work proposes a critical evaluation of the compatibility of a CAN to the requirements of the power electronics field and evaluates the recovery efficiency through mechanical and electrical indicators.

INDEX TERMS Epoxy, Integration, Power Module, Printed Circuit Board, Reliability, Self-healing, Vitrimers

I. INTRODUCTION

Power electronic modules based on Printed Circuit Board (PCB) with embedded active and passive components are solutions that can answer the requirements of higher integrability and efficiency, more effective cooling and simpler manufacturing, compared to the state-of-the art classical power modules based on DBC (Direct Bond Copper) substrates. [1]–[3]

To satisfy the requirements of PCB-embedded architectures, the dielectric surrounding the chip is now accountable for several new functions on top of its electrical insulation and environmental protection roles. It is now required to provide mechanical support to the module, acting as the main substrate, but also to play an active part in heat dissipation through the package, which was previously handled by the DBC's dielectric.

With such critical functions, the healthy condition of the encapsulation material becomes more and more important for the average lifespan of PCB-integrated power modules and such drastic changes bring several unknown factors in terms of reliability.

FR4 materials traditionally used for PCB applications are not designed to sustain harsh power cycles ($\Delta T > 120°C$), resulting in large thermal stresses and leading to mechanical failure [4], [5]. For integrated high-voltage power converters, such damages are likely to hamper the cooling capabilities (degraded thermal contact, burnout) and trigger electrical damage events (partial discharges, breakdowns) ultimately leading to device failure.

Thermal stress is often attributed to the mismatch in Coefficient of Thermal Expansion (CTE) between bonded materials subjected to temperature cycles. To better match the CTE of metals and ceramics contained in the stack, the general trend is to implement inorganic fillers into the dielectric, thus creating a composite of reduced CTE [6], [7]. Another popular route is to use polymers with high glass transition temperatures (Tg), as most polymers will exhibit a CTE increase past this transition [8].

However, thermal stress is not only tied to the CTE mismatch, but also relates to the stiffness of the participating materials. Increasing the filler content in glassy polymers does decrease the CTE mismatch but increases the overall stiffness of the dielectric, which may generate higher stresses for a given elastic strain [9].

In that regard, having a more compliant polymer as a matrix, capable of accepting a higher degree of deformation could be beneficial to improve the reliability of embedded electronics power boards [10].

But reliability is not solely related to the management of maximum stress peaks, as it is also defined in relation to the expected time of service. With the need to guarantee a reliable operation of modules for an ever-increasing amount of time, ensuring prolonged periods without failures seems quite challenging.

In that regard, developing new disruptive material concepts capable of recovering from past damages could be valuable from a reliability perspective. This approach could primarily help to reverse damage states back to a healthier situation but could also decrease the prevalence of failures by reducing the coupling between mechanical degradation and other induced failure modes (damage prevention approach).

Self-healing is the ability of a material to recover a set of properties from a degraded state. In the realm of self-healing materials, one can differentiate between extrinsic concepts that rely on external sources to provide the recovery effect, from intrinsic concepts that uses the inherent ability of the material to heal (i.e., its own physico-chemical properties) [11].

Recently, new self-healing materials have received a large scientific interest and are being actively researched with the intent to increase their use at the industrial scale [12]. These new materials called Covalent Adaptable Networks (CANs) offer intrinsic healing properties by dynamically exchanging covalent bonds between chains, similarly to supramolecular network using non-covalent bonds [13]. Among CANs, associative networks can perform this covalent bond exchange without depolymerization, keeping network continuity while rearranging their structure, effectively conserving the average crosslink density of the material [14].

By exchanging chain radicals, the network is not fixed anymore and accepts a degree of mobility that can be used to trigger material flow. This molecular-scale mobility allows to spread healing capabilities at any point within the volume and could theoretically reach infinite recovery cycling potential, provided that the chemical exchange equilibrium is not deteriorated by the aging of the material.

Among the most well-known CANs, transesterification-based materials (initially called vitrimers) can be synthesized from readily available commercial epoxy resins cured with carboxylic acids in the presence of a catalyst, making it a chemistry of choice for PCB-related applications [15]. This elaboration path allows to incorporate blends of reagents, making it very flexible for formulating new vitrimer materials for the field of electronics [16]. Transesterification is typically noticeable above 120-150 °C (kinetically limited) but can slowly start its exchange process at lower temperatures (thermodynamically limited) [17]. By being able to perform these exchanges at high rates at the expected operating temperatures of the next generation of power modules (up to 200 °C), the dielectric could be healed autonomously at each power cycle. Vitrimers are also known for their interesting viscoelastic and stress-relaxation properties, which are similar to the ones of silica glass from which the name vitrimer originated [18].

Overall, this new class of dielectric materials may open new opportunities to answer the challenging requirements of PCB-embedded power modules. Maintaining the overall crosslink density of a covalently bonded network is beneficial to the substrate function (mechanical support) of the board, while developing dynamic viscoelasticity allows to reduce the risk of mechanical failure. The prospect of a repetitive healing effect at the most stressed region, i.e. close to the power component also seems interesting from a reliability point of view.

However, for now vitrimers are mostly explored for structural applications and have not been tested in a stressful electrical environment. The compatibility of such materials is still to be demonstrated for power electronics applications and the majority of the electrical properties of these materials are still to be characterized and understood.

The objective of this work is to develop and test a vitrimer material to rate its compatibility for the development of auto-repairable PCBs for integrated power electronics. Ultimately, the goal is not to propose a fully optimized material, but rather to validate the concept and identify the opportunities and limiting factors that vitrimer materials can provide to the power electronics field.

This paper is organized as follows:

- First, the vitrimer elaboration and the sample manufacturing process are briefly explained.
- Then, the compatibility of the material with the application frame is evaluated. Given the novelty of such a material, priority was given to the most critical properties required from the neat matrix first (without inorganic fillers). As such, the dielectric strength, the thermal stability and the storage modulus of the neat material were assessed. Interesting new properties drawn from the dynamic network are also showcased and discussed in relation to embedded power electronics field.
- Finally, the self-healing behavior will be demonstrated for unreinforced and composite samples. The efficiency of the healing effect will be evaluated in mechanical and electrical tests, rating the expected confidence in the property recovery of previously damaged volumes.

II. VITRIMER ELABORATION

A. ELABORATION OF THE PRE-POLYMER RESIN

For this study, diglycidyl ether of bisphenol A (DGEBA – Epoxy equivalent = 178 $g.eq^{-1}$) and Sebacic Acid (SA 99 % purity – Acid equivalent = 101.13 $g.eq^{-1}$) were selected as the main precursors. For the catalyst, 1-Methylimidazole (1-MI 99 % purity) was used. All reagents were purchased from Sigma-Aldrich and used without further purification.

The elaboration process is based on Altuna et al.'s procedure [19]. All reagents were introduced in liquid phase, using a 10 % excess of epoxy to acid groups to ensure

completion of the reaction. The catalyst content was set to 5 % molar, also compared to acid groups.

B. CURING PROCESS AND CROSSLINKING

The curing reaction was followed by Differential Scanning Calorimetry (DSC) using a TA-DSC 2010 instrument, by introducing a small portion of the reagents and raising the temperature with similar heating parameters as in later manufacturing steps (14 °C/min from room temperature to 150 °C). After 20 min at 150 °C, no other heat exchanges could be observed (the test was stopped after 2 h). To ensure a sufficient reaction time in the press, the final curing time was therefore set at 1h for a curing temperature of 150 °C.

Following 1 hour of curing time at 150 °C, the conversion of the epoxy and carboxylic acid groups into the desired alcohol and ester groups was also verified by Fourier-Transform InfraRed spectroscopy, in Attenuated Total Reflectance configuration (ATR-FTIR).

To confirm the crosslinked nature of the final material, another DSC analysis was performed with a heating rate of 5 °C/min from 0 to 200 °C under a nitrogen gas atmosphere. As Figure 1 shows, the obtained thermograms display no further reaction or transition of the material up to 200 °C. The glass transition temperature was rated at 32 °C, at the curve onset of the cooling run (green circle) to avoid the first relaxation artefact (reversible physical aging – red circle).

All of these tests confirmed the complete curing of the material after 1 h at 150 °C.

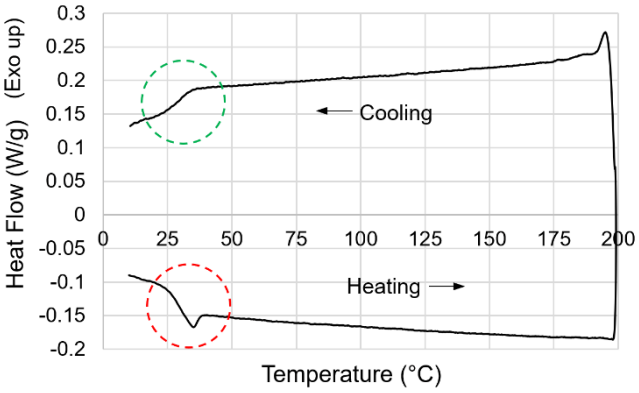

FIGURE 1. DSC thermogram of the elaborated vitrimer showing the specific heat jump at Tg (evaluation at green circle), showing an endothermic peak corresponding to the recovery of physical aging (red circle)

C. SAMPLE MANUFACTURING

Manufacturing of samples was achieved by hot-pressing using a LPKF Multi-Press S. A pressing vessel made of aluminium and steel plates was used to help with heat and pressure homogeneity.

To receive the pre-polymer, a sacrificial mold was designed using a layering of polytetrafluoroethylene (PTFE) unmolding sheets for top and bottom covers and an anti-adhesive spacer for the sides (sample thickness depends on the spacer used, from millimetric down to 100 µm thickness) (Fig. 2).

All samples from this study were made by filling this kind of sacrificial mold with resin and placing it inside the pressing vessel for later curing in the hot-press (150 °C – 1 h – 1 MPa).

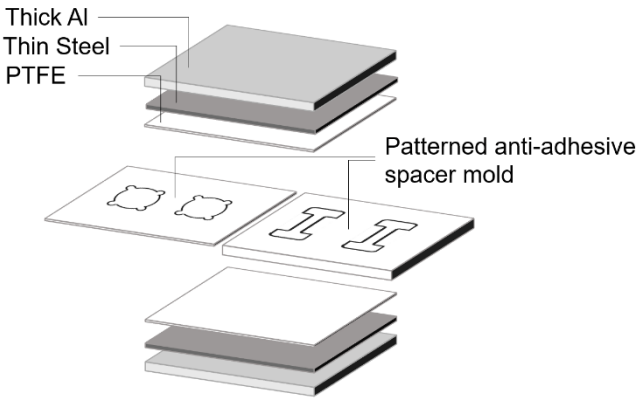

FIGURE 2. Pressing vessel (Al + Steel) and the sacrificial mold (top/bottom PTFE + custom spacer mold)

For composite samples using this self-healing matrix, fiberglass reinforcement was used. The glass cloth was precisely cut to size using a CO2 laser and laid inside the sacrificial mold. The hot pre-polymer was then directly poured onto the fibers before closing the mold and perform the hot-press curing as stated previously (150 °C – 1 h – 1 MPa).

For Resin Coated Copper (RCC) and PCB samples, the PTFE top and bottom sheets were replaced with 35 µm thick copper sheets, thus permanently bonding both copper layers to the resin contained within the mold. In this case, the spacer layer must be destroyed to recover the copper-layered samples. The copper sheets used for these samples are typically made for PCB manufacturing and are surface-treated (brown oxidation) to provide a mechanical anchor to the resin inside the rugosities.

III. KEY PROPERTIES FOR EMBEDDED POWER ELECTRONICS

A. NEAT MATRIX PROPERTIES

1) DIELECTRIC STRENGTH

As a primary specification for the electrical insulation of high voltage integrated devices, the dielectric strength of the elaborated vitrimer was assessed.

To rate the dielectric strength, breakdown tests were conducted at room temperature, using a Baur DPA-75C tester in a sphere-to-sphere configuration (1/2” diameter spheres). The electrical field is considered uniform in the sample.

Based on preliminary tests, an AC voltage (50 Hz) with a ramp of 2 kV/s was selected to obtain breakdowns between 10 and 20 seconds, thus limiting the electrical aging of the material.

Normalized breakdown test results can still vary depending on the thickness of the material (due to more defects in thicker pieces) [20]. Since a typical insulation layer for an embedded

module ranges in the hundreds of microns in thickness, 350 µm thick samples were used for this test.

To prevent flashover, the film samples were immersed in a fluorinated dielectric liquid (Galden HT55), with a dielectric strength of about 15 kV/mm.

A two-parameter (α and β) Weibull statistical analysis using Fothergill's median rank corrections [21] has been favored to statistically describe the breakdown results (Fig. 3).

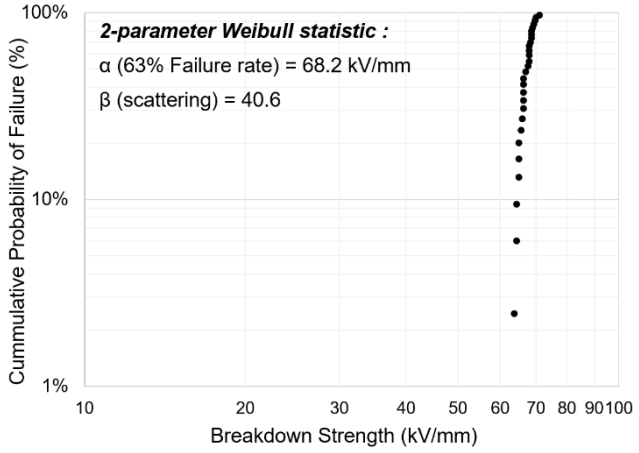

FIGURE 3. Weibull plot of the vitrimer breakdown strength showing the calculated alpha and beta parameters.

According to these data, the material presents a high dielectric strength at the chosen application-relevant thickness, with the lowest breakdown value being above 60 kV/mm and the highest being above 70 kV/mm. Focusing on the Weibull parameters, the data can indeed be represented as a two-parameter Weibull distribution (linear fitting) and the high beta values show a narrow distribution of results, with an alpha value above 68 kV/mm. This is comparable with the expected values for neat epoxy resin typically used in PCB manufacturing (about 50 kV/mm) [1].

In comparison, power modules based on new wide bandgap semiconductors are expected to have voltage ratings in the range of 10 kV, with thinner dielectric layers around the side of the chip (electric field > 10 kV/mm), but also thinner insulation on top of the component compared to Si-chip devices [22], [23].

In regard with the new advancements in terms of design geometries [24], field-grading materials [25] and the ability to tune the permittivity of the insulation [23], the dielectric strength of the vitrimer developed in this work is well aligned with the breakdown strength requirements of highly integrated designs (PCB-embedded) using wide bandgap technology.

2) THERMAL STABILITY

Thermal stability is another important specification for a PCB material, as the polymeric matrix can be exposed to high temperatures during solder operations (up to 270 °C in Lead-free processes).

To assess the thermal stability of the material, thermogravimetric analysis (TGA) was performed. To reflect the standardized tests that materials are subjected to in industrial environment, a protocol was designed around the ASTM D3850 standard.

Using a NETZSCH TG209 TGA/DTA analyzer, the thermal stability test was performed from room temperature to 700 °C, following a ramp of 10 °C/min, with a drying pause introduced at 150 °C for 15 min before continuing the heating ramp. Measurements were achieved both in pure nitrogen and in dry air to discriminate the effect of an oxidative environment on the material's mass loss.

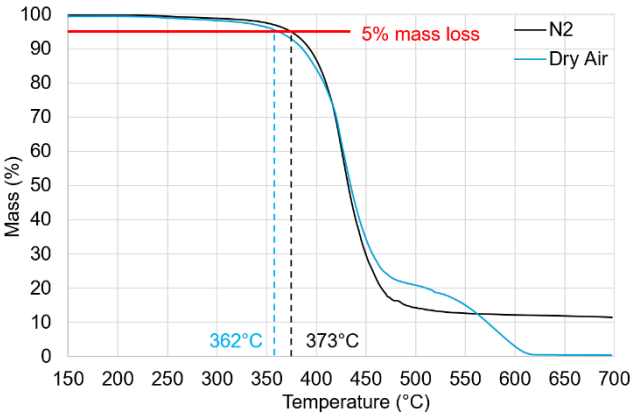

FIGURE 4. Vitrimer mass loss measurement associated with thermal degradations in pure nitrogen and dry air.

The data shown in Figure 4 was obtained continuously after the drying step at 150 °C. Since the mass loss is almost linear up to 350 °C, values were gathered by directly intersecting the 95 % ordinate of the curves (not the onset). A 5 % mass loss was recorded at 373 °C in pure nitrogen and at 362 °C in dry air.

One can notice the absence of impact of the oxygen partial pressure (pO2) in the 400-450 °C interval. This is due to the fact that phenolic-based polymers start to degrade by auto-oxidation, as several mechanistic pathways have been proposed in that direction [26], [27].

In normalized tests, most FR4 composite materials exhibit a mass loss of 5 % between 320 and 350 °C [8]. Considering the intermediate temperature of 288 °C typically used in PCB delamination tests, a mass loss of about 1 % was registered in dry air for the vitrimer matrix alone.

Given that the tested vitrimer is not reinforced and that no inorganic filler can increase the overall sample at all temperatures, one can expect an even higher rated thermal stability of vitrimer-based composites.

3) STORAGE MODULUS

A typical PCB also needs endure several pressing and lamination operations during its manufacturing, as well as other mechanical stresses when mounting components and attaching the board in the final device. Ensuring a sufficient elastic behavior is therefore valuable before implementing this resin into composite materials, that will further enhance the mechanical properties.

In order to measure the elastic properties of the material as a function of temperature, a Dynamic Mechanical Analysis (DMA) was performed in tensile configuration on parallelepipedal vitrimer bulk samples (10 x 5 x 2 mm3). Using a Mettler-Toledo DMA1, the scan was performed at 10 Hz with a temperature ramp of 2°C/min from 0 to 120 °C (Fig. 5).

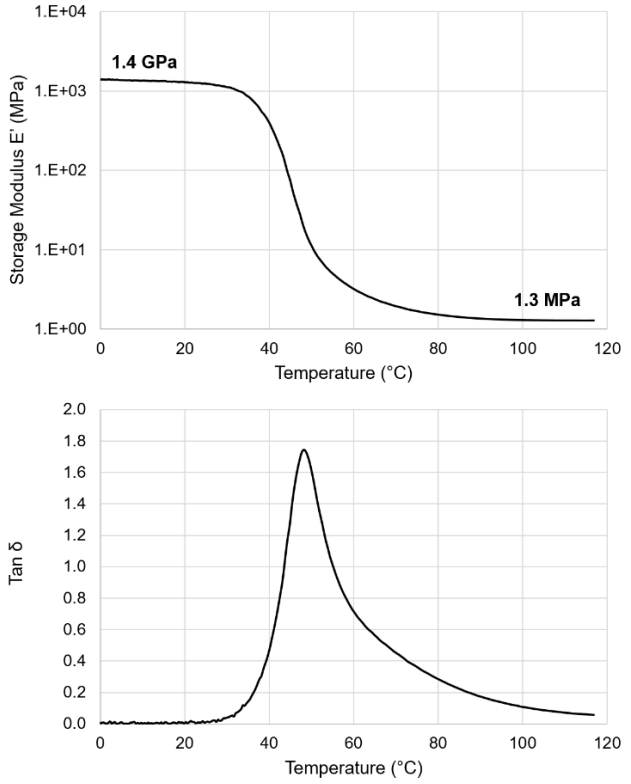

FIGURE 5. Top) Storage modulus of the elaborated vitrimer with temperature. Bottom) Associated loss factor.

According to these results, the elaborated vitrimer exhibits a storage modulus of 1.4 GPa below the glass transition temperature (Mechanical Tg = 35 °C, determined by E' onset), which is common for most unfilled epoxy compounds. However, a significant reduction can be observed above Tg, showing a much lower storage modulus of 1.3 MPa.

Looking at the loss factor values, the maximum mechanical damping can be found at 46 °C, but is severely skewed towards high temperatures. This effect may be attributed to the activation of the transesterification in the material, which is known to generate viscoelastic effects [17].

According to this test, manufacturing and manipulation of vitrimer-based PCBs below Tg should be reasonably achievable in an industrial environment. The rather high modulus depicts a hard/glassy material that can be employed for its structural support, comparable with other unfilled epoxies. Above Tg however, the material becomes much softer and is best described as a rubber, which may require reinforcements in order to assume a mechanical support role. Still, in practice, it is possible to manipulate the material with little integrity concerns even above Tg, as the vitrimer rubber is sufficiently tough and appears to remain stable in dimensions. However, mechanically challenging operations should be reserved for temperatures below Tg or be adapted accordingly for higher temperatures.

To address a typical concern that might arise from the low-Tg and the expected increase of the CTE, one should consider that thermal stress is related to both the CTE and the elastic modulus (stiffness term). While CTE evaluation was not performed in this study, it is unlikely that its increase past Tg would overcome such a large decrease in modulus (three orders of magnitude). With appropriate dimensional design considerations, it is possible that this material would produce less thermal stress at high temperatures by being the most compliant participant of the stack.

B. COMPARISON WITH A COMMERCIAL REFERENCE

1) COMPOSITE MANUFACTURING

To compare this new dielectric with state-of-the-art prepregs used in the PCB field, fiberglass reinforced samples were produced.

Since glass fibers can be found in many weaving types, a fair comparison can only be obtained with materials of the exact same reinforcement.

For this study, a high-performance commercial reference using E-rated 1080 glass cloth was selected (Isola 370HR prepregs) and cured according to the manufacturer's recommendations. For the vitrimer composites, an identical reinforcing glass cloth was selected, and the composite piece was manufactured using conditions presented in part II.C.

A comparison of both composite samples is available in Figure 6, showing similar cross-sections.

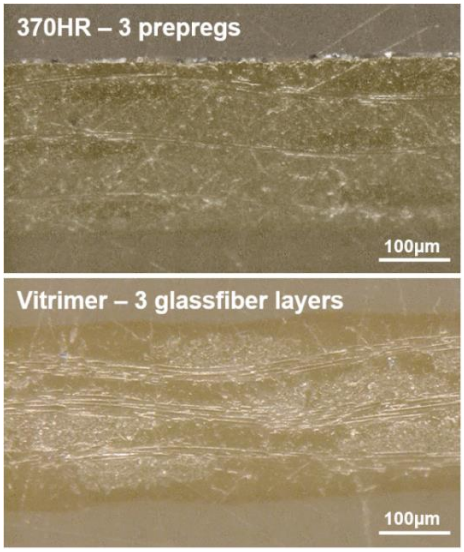

FIGURE 6. Cross-sections of two composite samples. Top) 370HR commercial reference (3x prepregs). Bottom) Vitrimer composite (3x 1080 E-glass cloth layers)

2) COMPOSITE CHARACTERIZATION

To measure the elastic properties of both composites, DMA was performed again with a Mettler-Toledo DMA1 in tensile configuration, on the welft axis of the composite samples (10 x 5 x 0.35 mm3). The test was run under an oscillating load of 2N at 10 Hz, with a temperature ramp of 2.5 °C/min from 0 to 300 °C.

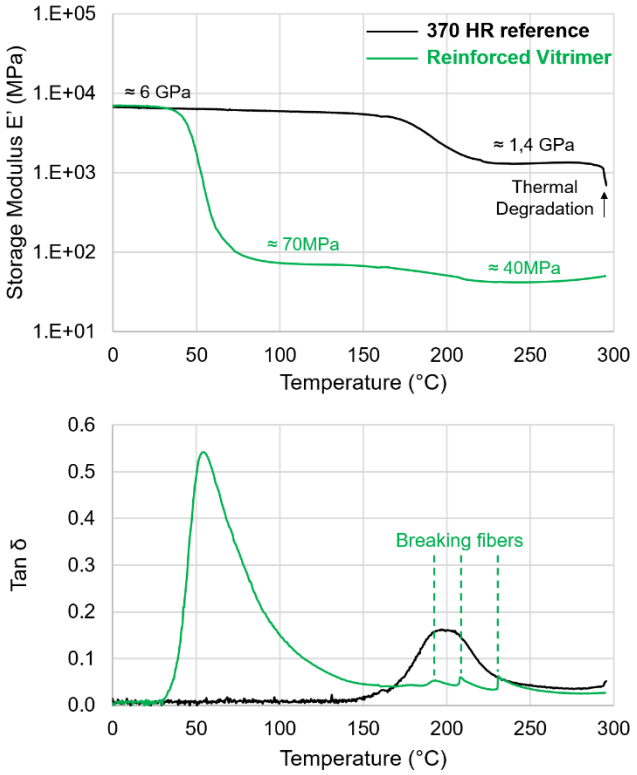

FIGURE 7. Top) Storage modulus comparison between the 370HR reference and the elaborated vitrimer with temperature. Bottom) Associated loss factor.

Results for the storage modulus and mechanical losses can be found in Figure 7. The vitrimer composite shows the same storage modulus as the commercial reference below Tg (6 GPa – mostly controlled by the reinforcing material). However, the large modulus drop previously observed on the neat matrix is conserved even if mitigated by the reinforcement, making the vitrimer composite much more compliant than the 370HR in its rubbery state (70 MPa vs. 1.4 GPa).

As with the neat matrix, the vitrimer composite conserved an important mechanical loss peak skewed towards high temperatures, with a relatively high intensity compared to the mechanical damping shown on the 370HR reference.

Since this test was performed in load control, as the vitrimer matrix became more and more compliant, higher stresses were reported onto the fibers (representing a much smaller sample section) that started to break near 200 °C which further reduced the storage modulus (down to 40 MPa). However, this effect was entirely related to the test conditions.

Observation of the samples before and after this test are available in Figure 8. The vitrimer material is more stable than the commercial reference at high temperatures, even though both materials are rated for such a temperature range. While the vitrimer darkened significantly as it is expected for epoxies in hot oxidative environments, the 370HR composite almost entirely burned out, which can be observed by a fall in the storage modulus near 300°C.

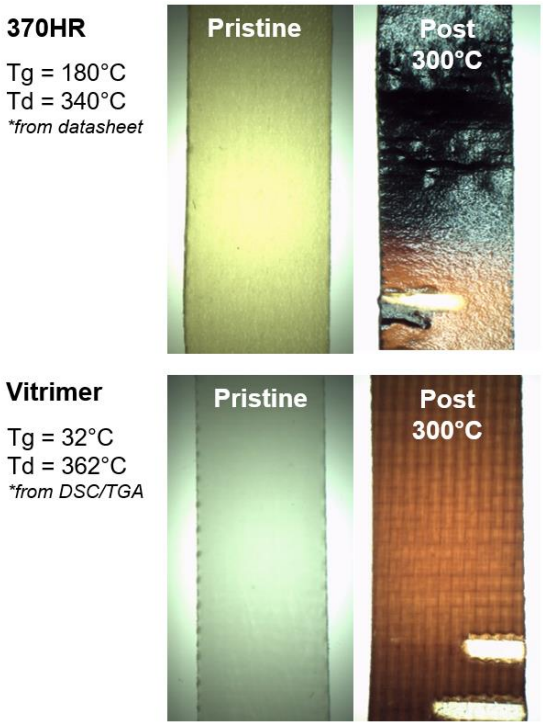

FIGURE 8. Observations before/after testing both materials up to high temperatures (DMA – up to 300° C).

This test demonstrates that reinforcing a vitrimer is a valid path for improving its mechanical properties, even above Tg, while conserving a large degree of compliance and mechanical damping. These results also show that vitrimer composites can be stable at high temperature, even though their glass transition temperature is low compared to standard materials. Overall, modifying the mechanical properties of vitrimer composites is possible to increase their compatibility with manufacturing constraints.

C. DYNAMIC NETWORK PROPERTIES

1) STRESS-RELAXATION

Vitrimers are known for their interesting viscoelastic behavior and evaluating these time-related properties through stress-relaxation experiments has now been accepted as a suitable mean to study the network mobility (i.e., the dynamic exchanges responsible for the self-healing behaviour) [28]. Put aside the self-healing potential of the material, evaluating the ability of these materials to relax stress is valuable in itself for highly integrated systems that endure large stresses and would benefit directly from mechanical relaxations.

To evaluate relaxation capabilities of the formulated materials, stress-relaxation tests were performed, using a

Mettler-Toledo DMA1 operated in tensile mode on unreinforced parallelepipedal bulk samples (10 x 5 x 2 mm3). The samples were submitted to a constant strain of 5 % in isothermal conditions and the stress response was measured as a function of time for 1 hour. The tests were performed from 100 °C and up to 175°C, following incremental isothermal steps of 25 °C.

The relaxation time τ of the vitrimer matrix was determined by fitting the stress relaxation data with a simple exponential function, as proposed in Maxwell's viscoelastic model as follow in Equation 1:

$$\sigma_t/\sigma_0 = e^{-\frac{t}{\tau}} \qquad (1)$$

The fitting was performed only up to 63 % relaxed stress (dashed horizontal lines in Figure 9) to ensure that it is not impacted by experimental deviation from exponential behavior when the measured relaxing load becomes low (when σt/σ0 < 37%). All relaxation times from Table 1 were calculated using the exponential factor of the best fitted exponential function (Fig. 9).

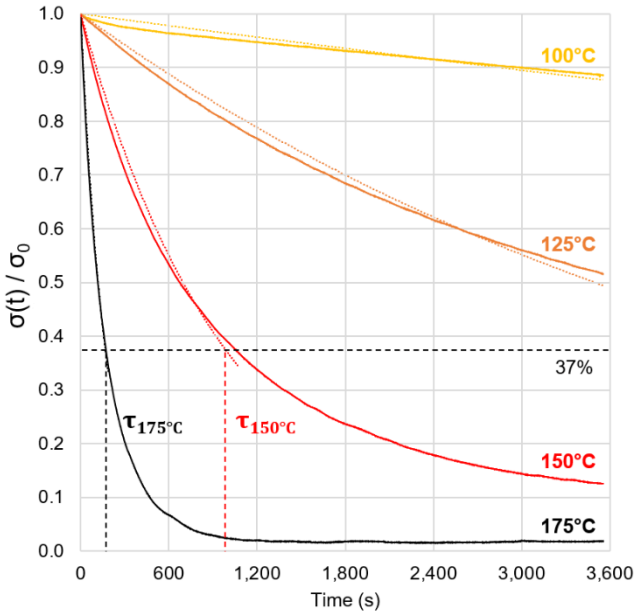

FIGURE 9. Isothermal stress relaxation experiments with exponential fittings (dotted lines) showing stress decrease as a function of time (graphical τ determination is only shown for illustration purposes).

As shown in Figure 9, a significant decrease of the initial stress applied to the vitrimer samples can be observed as a function of time above 100 °C. By increasing the temperature, the relaxation occurs faster. By heating the material at 150 °C, an almost complete stress relaxation can be reached in 1 hour (about 90% stress decrease), yielding a mostly stress-free material. At 175 °C, a completely stress-free state is reached in about 20 min.

Table 1 presents the relaxation times τ associated with each isothermal curve. Plotting each relaxation time as a function of reciprocal temperature will draw an exponential trendline that is known to follow an Arrhenius law in the appropriate plot. This is because the viscoelastic effects are directly related to the transesterification exchanges within the network, of which the kinetics also obey an Arrhenius law. By increasing the temperature, the exchanges are performed faster and the network is able to adopt a new configuration of lower stress in a shorter duration.

TABLE 1 – RELAXATION TIMES OBTAINED FROM ISOTHERMAL STRESS-RELAXATION CURVES EXPONENTIAL FITTING.

T(°C)	τ(s)	τ/τ175°C
100	27 115	160
125	5 048	30
150	1 004	6
175	169	1

This effect becomes macroscopically significant with increasing temperatures but can possibly start as soon as the vitrimeric transition temperature Tv is crossed. Indeed, similarly to the glass transition temperature Tg, which governs the physical mobility of chains in the network, Tv governs the chemical mobility of chains via transesterification. In order for the mobility of the network to be observed, both mobility limitations must be lifted.

In the applicative case of embedded power modules, it is clear that the relaxation of stress could happen during the power cycles, especially nearby the power component where an important temperature gradient can be found. This could guarantee the highest degree of stress-relaxation right in the most stressed areas, where the temperature is the highest, and remain moderately activated or inactivated in cooler parts of the module.

2) REPROGRAMMABLE SHAPE MEMORY AND RECYCLING POTENTIAL

Typical shape memory is mostly resulting from an out-of-balance deformed state that was imparted to the network above Tg before quenching it below Tg, thus preventing the chain network from relaxing internal stresses. When sufficient heat is provided, the network is able to relax and recovers its initial stress-free topology, which can be used as a form of mechanical work storage. In this regard, typical shape-memory is actually more related to a shape relaxation.

For vitrimers however, an interesting side-effect of the dynamic network is that it is possible to reach a stress-free state without reverting to the initial shape, as shown in stress-relaxation experiments, where a constant strain still leads to a stress-free state (section III.C.1). Thus, by simultaneously heating and deforming the material for a sufficient amount of time, it is possible to impart an entirely new relaxed shape to the material.

This side-effect can be useful in manufacturing operations, such as relaxation of bonded layers after the curing but could also be used to reshape the material after its elaboration.

Thus, by unlocking the ability to remodel their shape after the curing of the network, these crosslinked materials now become eligible for recycling, opening opportunities in terms of sustainability of electronics and other thermoset-based products.

Ultimately, this dynamic network could benefit from processing opportunities previously reserved to thermoplastics, making it a valuable technology to develop for many applications.

IV. EVALUATION OF THE HEALING EFFICIENCY

A. A. QUALITATIVE TESTS

As mentioned previously, recovery requires a mobile phase to fill damages and create the opportunity for healing. For large defects, a suitable recovery can be observed by combining the shape memory effects (macroscopic mobility) with the molecular exchanges (microscopic mobility).

As shown in Figure 10, a vitrimer film was repetitively bent below Tg until cracks started to appear. By heating the material above its Tg, the macroscopic mobility of chains is allowed, triggering regular shape memory effects (or shape relaxation). The entropy energy stored in the material is released as mechanical work in the deformed yet unbroken parts, which reduces the gaps in the failed material [29].

Once the failed surfaces are in contact, the transesterification between chains may start as soon as sufficient heat was provided (above Tv) and is sped up by increasing the temperature until an acceptable exchange rate is reached.

By doing so, one is actively setting a new stable network configuration across the failed gaps, effectively undistinguishable from the initial network. Thus, by modulating the heating profile, one could obtain material healing results without having to intervene directly inside the package.

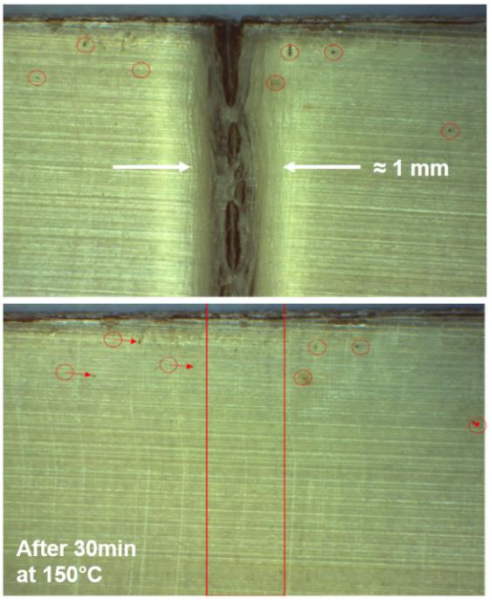

FIGURE 10. Qualitative demonstration of healing of a 300 µm thick unreinforced sample after mechanical fatigue failure.

It is also possible to obtain similar results with composite materials (Fig. 11). By applying a tensile stress with a 45° angle in respect to the direction of the reinforcements, interfacial defects were produced inside the material. By reheating the material for 1h at 150°C (above Tg and Tv), chain mobility is fully enabled and allows to entirely recover visible damages. In this case the damages were local delamination at the polymer-fiber interfaces.

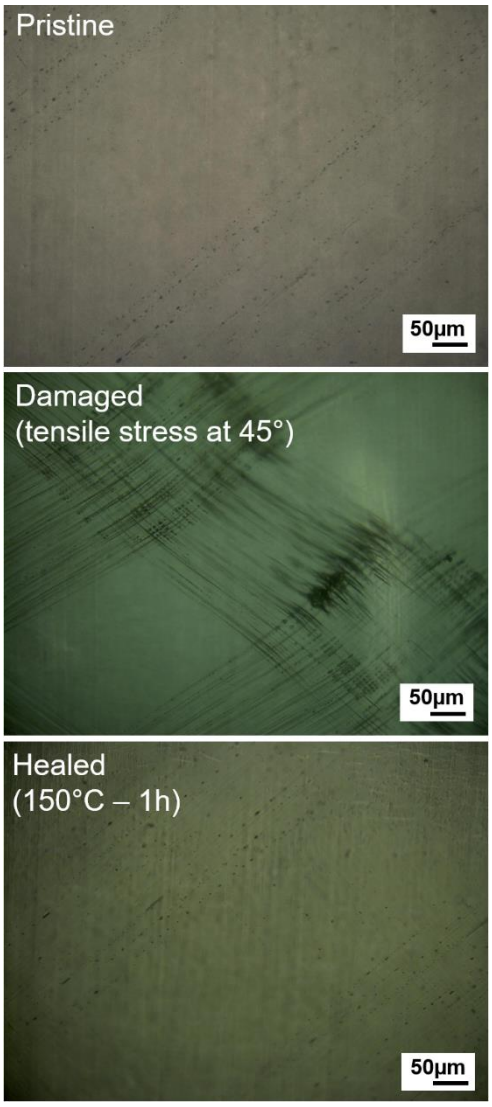

FIGURE 11. Qualitative demonstration of healing composite material after creating interfacial defects (tensile stress at a 45° angle from the reinforcement orientation).

B. HEALING EFFICIENCY AND RECOVERY PROTOCOL

Evaluating the extent of healing by simple crack closure observations is not sufficient to guarantee that the material will perform according to specifications. Rating the healing efficiency is typically made by measuring a given property

from a pristine sample and comparing it to the same property on a failed, then healed sample.

A comparison is often made between a new sample and a "reprocessed sample", obtained by recovering broken pieces and undergoing the hot-press manufacturing step again (similar to a recycled sample) [16], [30], [31]. This reprocessing usually involves the application of large pressures to help merging pieces together, which is not representative of what can happen inside of a closed power semiconductor package in operation. A more suitable healing evaluation for this topic would mainly rely on heat to achieve the healing process without any external force applied during healing. Also, as discussed previously, using the shape memory properties of the material can still allow to create an internal form of pressure without external interaction.

Therefore, as a recovery test protocol oriented towards conditions for self-healing in operation, all broken samples were subjected to a shape recovery step (1 min – 150 °C) to trigger the shape memory of the material, followed by a healing step (1 h – 150 °C).

For entirely severed samples, as in tensile tests (section IV.C), manual positioning is provided to bring pieces into contact with the minimal amount of force required, before letting them free to heal in the oven. For partially severed samples, as in breakdown tests (section IV.D.2), the shape memory effect was often sufficient to achieve the same result autonomously and manual intervention was only performed when absolutely necessary.

C. MECHANICAL TEST

To rate the extent of the recovery on mechanical properties, a simple test procedure was followed. First, two dumbbell-shaped samples were tested on a tensile mechanical bench until complete failure. Then, the sample pieces were gathered and followed the recovery protocol. Finally, the healed samples were tested again under the same conditions, as it is possible to destructively test the same sample several times.

The samples were obtained by creating a new 2mm thick mold, using a scaled down version of the ASTM D638-14 standard type IV dumbbell design (85 mm length).

To reset the thermal history prior to the first test, all samples were heated for 10 min at 150°C and cooled down to room temperature. After the recovery step, the healed samples were tested immediately.

A Mecmesin Multitest-i bench was used in tensile configuration, and performed at a strain rate of 20 mm/min at room temperature.

Figure 12 shows the results for two pristine and healed samples (S01 & S02). Both pristine samples exhibited similar elastic domains, with a toe region at the beginning and linear portion up until yielding. Similar strength at yield was recorded and both plastic deformations led to a rather steady deformation plateau until ultimate failure after about 25% strain.

After the recovery protocol, both healed samples also showed a very similar mechanical profile in the elastic region, with equivalent elastic modulus and maximum strength before failing near the 10% elongation mark.

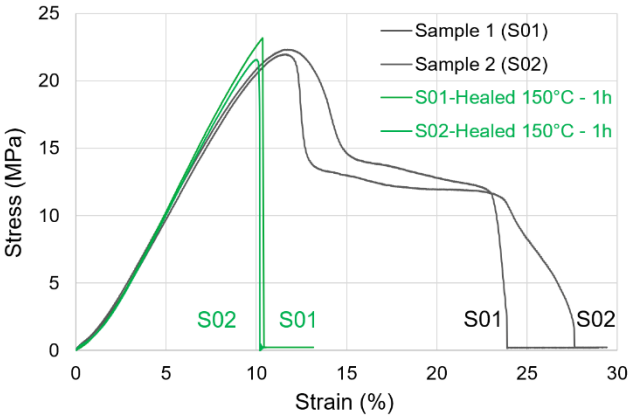

FIGURE 12. Tensile test performed to failure twice on the same two samples, showing the recovery of most elastic properties after the healing protocol.

By comparing the pristine and healed data sets, one can observe a similar elastic domain, with an almost complete recovery of the elastic modulus as well as the maximum strength.

Although the yielding of the healed network occurred roughly at the same stress and elongation as for the pristine materials, the subsequent failure mechanism changed from a ductile to a fragile mode and occurred at the exact previously failed location on the samples. This indicates that the test was measuring the strength of an imperfect adhesive joint that acted as a guide for new crack propagation and yielded abruptly before the plastic deformation of the material.

Overall, it is not usually expected from a material to perform near its plastic domain, meaning that the healed material should be able to endure reasonable elastic stresses that a pristine matrix is designed to endure in operation. However, this might indicate that the healing protocol could be improved to produce a more intimate joint between both networks.

D. ELECTRICAL TEST

1) TEST CONCEPT

As a second part of this study, a similar recovery test was designed to verify that the healed region could withstand high electrical fields.

Indeed, mechanical damages can decrease the breakdown strength of the insulating material, by reducing the overall thickness or by creating initiation sites for partial discharges, which will erode the material and trigger a breakdown after some time. Therefore, the purpose of this test is not to repair a dielectric breakdown but to evaluate the rate of recovery of the breakdown resistance in repaired volumes.

To evaluate the breakdown voltage recovery, specific samples had to be designed, concentrating both mechanical and electrical stresses in the same region.

Using the manufacturing protocol detailed in II.C, a dual sided Resin Coated Copper (RCC) sample was produced. The obtained RCC quality was satisfying, with homogeneous and adequate thicknesses for each layer and no observable voids (Fig. 13).

The RCC was then selectively etched using only conventional PCB manufacturing methods (dry film lamination, masking, UV exposition, chemical etching etc.), demonstrating the practical ability to make printed boards even without reinforcement.

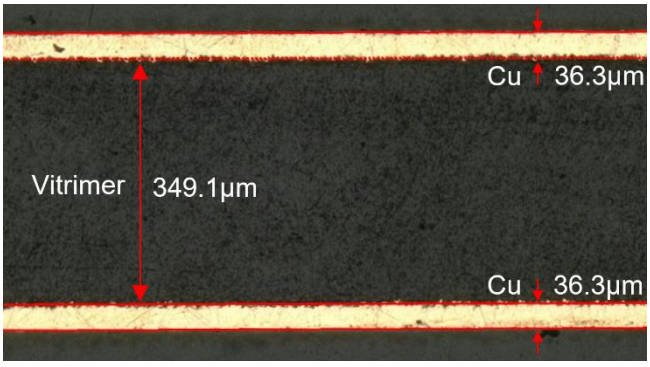

FIGURE 13. Cross-section of a self-healing RCC manufactured by hot-press molding.

For electrical stress concentration, the PCB was patterned with field-enhancing electrode tips separated by each other with a controlled 1mm gap. To fully insulate the electrodes, the entire board was encapsulated in a new batch of the polymer.

For mechanical stress concentration, notches were made to initiate and channel cracks in between the electrodes. An open void notch was used to stop the propagation of the crack before totally severing the sample. This allowed to keep a small portion of the polymer intact and take advantage of the polymer shape memory to precisely self-realign the electrodes during the recovery process (Fig. 14).

A total of twelve samples could be made on a single 10x15 cm^2 board simultaneously, enhancing the repeatability of the test. A CO2 laser ablation was used to remove some of the polymer for electrical contacts and cut the notches for all samples in one operation, effectively demonstrating the possibility to create vias using lasers at a panel-level processing.

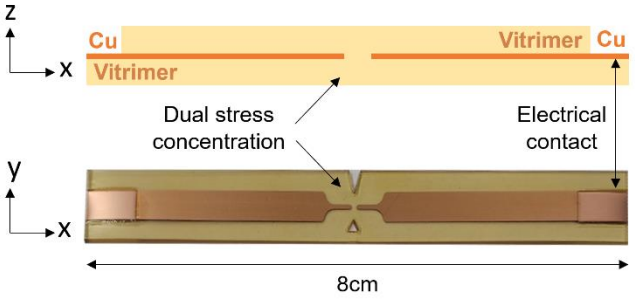

FIGURE 14. Sample design for breakdown recovery tests, showing the dual stress concentration region.

2) BREAKDOWN STRENGTH RECOVERY TEST

For this test, a baseline was set by measuring the inherent dielectric breakdown voltage of a group of pristine, undamaged samples. Three other groups of samples were damaged mechanically before undergoing the healing protocol at 150 °C, with an increasing healing duration of 5 min, 30 min and 1 h for each group. After the end of each recovery duration, samples were cooled down to room temperature and tested on the dielectric breakdown bench immediately.

Introducing a mechanical damage creates significant geometrical changes to the sample. Thus, evaluating the breakdown strength right after the damage step is not a representative test, since the result will depend on the electrode distance, isolating fluid, and fractured geometry. The healing efficiency of the vitrimer is therefore evaluated by comparing the evolution of breakdown strength distributions between samples healed at different durations. In this case, the samples geometry is the same as the pristine sample, and the effect of the isolating fluid can be neglected.

Mechanical damages were produced with a Deben Microtest tensile stage at a strain rate of 1mm/min at 20 °C. The stage was stopped after the crack had propagated up to the open triangular void, i.e., before complete severing of the sample.

Breakdown strength tests were performed in the same conditions and apparatus as described in section III.A.1 using a 2 kV/s AC voltage ramp at 50 Hz.

A summary of the experimental protocol can be found in Figure 15.

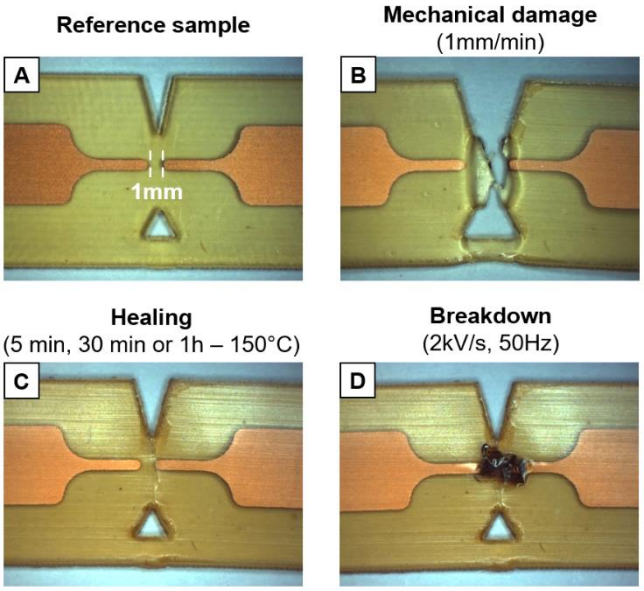

FIGURE 15. Experimental steps used in the breakdown voltage recovery tests.

Figure 16 compares the average breakdown voltages of unbroken samples (Reference) with broken and repaired samples (Healed) that experienced different recovery times (from 5 min to 1 h) at 150 °C. Error bars represent the standard deviation for each data set.

After only 5 min at 150°C, a high recovery of the breakdown strength was already registered, with an average 85 % of the pristine breakdown voltage value, albeit with a very large dispersion of results. After 1 h however, the recovery increased to virtually 100 %, sharing the same dispersion of results as for the reference samples.

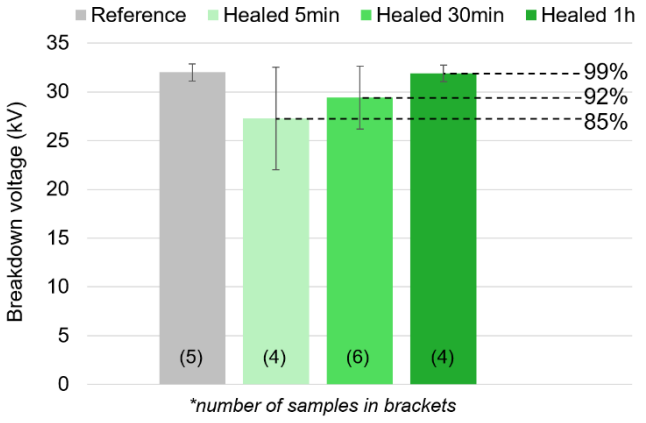

FIGURE 16. Breakdown voltage recovery results for undamaged references (grey) and broken/healed samples (green).

This data shows a high recovery rate of the average breakdown strength likely resulting from the recovery of mechanical damages. A large portion of breakdown voltage was recovered rather quickly, with the lowest data point for the "Healed 5min" data set being registered at 21 kV/mm. By increasing the healing time, the remaining defects within the material could be healed, which translated into an improvement of the value of the breakdown voltage but also as a reduction of the overall dispersion. This shows that improving the healing protocol can provide better healing efficiency results and limit the risk of incompletely recovered regions that would decrease the material breakdown voltage under electrical stress conditions.

V. CONCLUSION

Vitrimers are promising materials for future applications as a highly-stressed power semiconductor insulating packaging material.

The material formulated in this study is compatible with the basic requirements of high-power integrated devices. With a high dielectric strength and thermal stability, and a reasonably high storage modulus, it is possible to envision this material inside a working embedded power module.

Although it is favorable to manipulate the material below its glass-transition temperature to benefit from the higher mechanical properties, it should still possible to work at higher temperatures, either by adapting the manufacturing process or by using reinforcement fillers. Further tuning of the properties is also possible, notably for changing the Tg and Tv of the material to modify its thermomechanical characteristics.

The self-healing behavior was demonstrated, explaining the effects allowing the mobility of the network required for healing. The ability to relax stress mechanically by increasing the temperature was shown and this could be exploited to selectively alleviate stress in hot spots while maintaining a higher rigidity away from power semiconductors dies (i.e. in cooler parts of the module).

The healing efficiency was also explored with mechanical and electrical indicators, demonstrating a high degree of confidence in the recovery of property in the failed volumes after 1h at 150°C.

This study also demonstrated the manufacturing capabilities for bulk, film, reinforced, RCC and PCB samples using processing methods from the field of electronic PCB manufacturing. As a direct comparison with other composites, fiberglass cloth reinforced vitrimers could compete with high-performance references available on the market. With similar storage modulus below Tg, the vitrimer composite still showed a much larger compliance and mechanical damping capabilities above Tg, but also a much higher thermal stability compared to its commercial counterpart.

Overall, this class of materials is adaptable from a large selection of commercial resin systems, offering a large range of formulation potential making it adaptable for targeted applications. Additionally, the added benefits of the dynamic network, such as self-healing, reprogrammable shape-memory and recycling open numerous new opportunities that can be beneficial to develop durable and more sustainable power electronic packaging systems.

VI. References

[1] T. Huesgen, « Printed circuit board embedded power semiconductors: A technology review », *Power Electron. Devices Compon.*, vol. 3, no 100017, p.1-15, oct. 2022, doi: 10.1016/j.pedc.2022.100017.

[2] F. Hou et al., « Fan-Out Panel-Level PCB-Embedded SiC Power MOSFETs Packaging », *IEEE J. Emerg. Sel. Top. Power Electron.*, vol. 8, no 1, p. 367-380, mars 2020, doi: 10.1109/JESTPE.2019.2952238.

[3] D. J. Kearney, S. Kicin, E. Bianda, et A. Krivda, « PCB Embedded Semiconductors for Low-Voltage Power Electronic Applications », *IEEE Trans. Compon. Packag. Manuf. Technol.*, vol. 7, no 3, p. 387-395, mars 2017, doi: 10.1109/TCPMT.2017.2651646.

[4] R. Randoll, W. Wondrak, et A. Schletz, « Dielectric strength and thermal performance of PCB-embedded power electronics », Microelectron. Reliab., vol. 54, no 9-10, p. 1872-1876, sept. 2014, doi: 10.1016/j.microrel.2014.07.139.

[5] M. Guyenot, D. Maas, R. Ratchev, A. Khoshamouz, T. Gottwald, et S. Kreuer, « New Failure Mechanism in High Temperature Resin Materials », I*EEE 68th Electronic Components and Technology Conference (ECTC)*, San Diego, CA, USA, 2018, p. 1238-1244. doi: 10.1109/ECTC.2018.00191.

[6] G. Li et al., « Mesoporous Silica Nanoparticles: A Potential Inorganic Filler to Prepare Polymer Composites with Low CTE and Low Modulus for Electronic Packaging Applications », *IEEE 66th Electronic Components and Technology Conference (ECTC)*, Las Vegas, NV, USA, 2016, p. 2134-2139. doi: 10.1109/ECTC.2016.176.

[7] W. Zhang, P. Zhu, T. Zhao, R. Sun, et C. Wong, « A study of underfill using two kinds of silica as inorganic filler », *14th International Conference on Electronic Packaging Technology*, Dalian, China, 2013, p. 296-300. doi: 10.1109/ICEPT.2013.6756475.

[8] C. F. Coombs, "Chapter 6 – Introduction to base materials" in *Printed circuits handbook*, 6th ed. in McGraw-Hill handbooks. New York, USA, McGraw-Hill, 2008, part3, ch. 6, p. 9-12.

[9] Y. W. Pok, D. Sujan, M. E. Rahman, et S. S. Dol, « Effect of Bond Layer Properties to Thermo-Mechanical Stresses in Flip Chip Packaging », *MATEC Web Conf.*, vol. 95, no. 01003, p1-6; 2017, doi: 10.1051/matecconf/20179501003.

[10] P. Lall, K. Dornala, J. Deep, et R. Lowe, « Measurement and Prediction of Interface Crack Growth at the PCB-Epoxy Interfaces Under High-G Mechanical Shock », *17th IEEE Intersociety Conference on Thermal and Thermomechanical Phenomena in Electronic Systems (ITherm)*, San Diego, CA, USA, 2018, p. 1097-1105, doi: 10.1109/ITHERM.2018.8419571.

[11] M. D. Hager, "Self-healing Materials", in H*andbook of Solid State Chemistry*, 1st ed., Wiley-VCH Verlag GmbH & Co. KGaA, 2017, ch. 9, p.201-225.

[12] V. Schenk, K. Labastie, M. Destarac, P. Olivier, et M. Guerre, « Vitrimer composites: current status and future challenges », *Mater. Adv.*, vol. 3, p. 8012-8029, 2022, doi: 10.1039/D2MA00654E.

[13] J. M. Winne, L. Leibler, et F. E. Du Prez, « Dynamic covalent chemistry in polymer networks: a mechanistic perspective », *Polym. Chem.*, vol. 10, p. 6091-6108, 2019, doi: 10.1039/C9PY01260E.

[14] N. J. Van Zee et R. Nicolaÿ, « Vitrimers: Permanently crosslinked polymers with dynamic network topology », *Prog. Polym. Sci.*, vol. 104, no. 101233, p. 1-12, may 2020, doi: 10.1016/j.progpolymsci.2020.101233.

[15] D. Montarnal, M. Capelot, F. Tournilhac, et L. Leibler, « Silica-Like Malleable Materials from Permanent Organic Networks », *Science*, vol. 334, no 6058, p. 965-968, nov. 2011, doi: 10.1126/science.1212648.

[16] J.-H. Chen, X.-P. An, Y.-D. Li, M. Wang, et J.-B. Zeng, « Reprocessible Epoxy Networks with Tunable Physical Properties: Synthesis, Stress Relaxation and Recyclability », *Chin. J. Polym. Sci.*, vol. 36, no 5, p. 641-648, may 2018, doi: 10.1007/s10118-018-2027-9.

[17] M. Capelot, M. M. Unterlass, F. Tournilhac, et L. Leibler, « Catalytic Control of the Vitrimer Glass Transition », *ACS Macro Lett.*, vol. 1, no 7, p. 789-792, july. 2012, doi: 10.1021/mz300239f.

[18] W. Denissen, J. M. Winne, et F. E. Du Prez, « Vitrimers: permanent organic networks with glass-like fluidity », *Chem. Sci.*, vol. 7, no 1, p. 30-38, 2016, doi: 10.1039/C5SC02223A.

[19] F. I. Altuna, C. E. Hoppe, et R. J. J. Williams, « Shape memory epoxy vitrimers based on DGEBA crosslinked with dicarboxylic acids and their blends with citric acid », *RSC Adv.*, vol. 6, no 91, p. 88647-88655, 2016, doi: 10.1039/C6RA18010H.

[20] B. Helgee et P. Bjellheim, « Electric breakdown strength of aromatic polymers: dependence on film thickness and chemical structure », *IEEE Trans. Electr. Insul.*, vol. 26, no 6, p. 1147-1152, dec. 1991, doi: 10.1109/14.108152.

[21] J. C. Fothergill, « Estimating the cumulative probability of failure data points to be plotted on Weibull and other probability paper », *IEEE Trans. Electr. Insul.*, vol. 25, no 3, p. 489-492, june 1990, doi: 10.1109/14.55721.

[22] C. M. DiMarino, B. Mouawad, C. M. Johnson, D. Boroyevich, et R. Burgos, « 10-kV SiC MOSFET Power Module with Reduced Common-Mode Noise and Electric Field », *IEEE Trans. Power Electron.*, vol. 35, no 6, p. 6050-6060, june 2020, doi: 10.1109/TPEL.2019.2952633.

[23] J. Schuderer, U. Vemulapati, et F. Traub, « Packaging SiC power semiconductors – Challenges, technologies and strategies », *IEEE Workshop on Wide Bandgap Power Devices and Applications*, Knoxville, TN, USA, 2014, p. 18-23. doi: 10.1109/WiPDA.2014.6964616.

[24] M. M. Tousi et M. Ghassemi, « Characterization of Nonlinear Field-Dependent Conductivity Layer Coupled with Protruding Substrate to Address High Electric Field Issue Within High-Voltage High-Density Wide Bandgap Power Modules », *IEEE J. Emerg. Sel. Top. Power Electron.*, vol. 8, no 1, p. 343-350, march 2020, doi: 10.1109/JESTPE.2019.2953145.

[25] S. Diaham et al.,« Field Grading Composites Tailored by Electrophoresis-Part 3: Application to Power Electronics Modules Encapsulation », *IEEE Transactions on Dielectrics and Electrical Insulation*, 2021, vol. 28, no. 2, p.348-354, doi: 10.1109/TDEI.2020.009032.

[26] H. Jiang et al., « The pyrolysis mechanism of phenol formaldehyde resin », *Polym. Degrad. Stab.*, vol. 97, no 8, p. 1527-1533, aug. 2012, doi: 10.1016/j.polymdegradstab.2012.04.016.

[27] L. Costa, L. R. di Montelera, G. Camino, E. D. Weil, et E. M. Pearce, « Structure-charring relationship in phenol-formaldehyde type resins », *Polym. Degrad. Stab.*, vol. 56, no 1, p. 23-35, apr. 1997, doi: 10.1016/S0141-3910(96)00171-1.

[28] C. Taplan, M. Guerre, J. M. Winne, et F. E. Du Prez, « Fast processing of highly crosslinked, low-viscosity vitrimers », *Mater. Horiz.*, vol. 7, no. 1, p. 104-110, 2020, doi: 10.1039/C9MH01062A.

[29] V. Montano, M. W. Urban, S. van der Zwaag, et S. J. Garcia, « Local strain-induced energy storage as driving force for autogenous scratch closure », *J. Mater. Chem. A*, vol. 10, no 13, p. 7073-7081, 2022, doi: 10.1039/D1TA10441A.

[30] Z. Song, Z. Wang, et S. Cai, « Mechanics of vitrimer with hybrid networks », *Mech. Mater.*, vol. 153, no. 103687, p. 1-12, feb. 2021, doi: 10.1016/j.mechmat.2020.103687.

[31] H. Zhang et al., « Recyclable Polydimethylsiloxane Network Crosslinked by Dynamic Transesterification Reaction », *Sci. Rep.*, vol. 7, no 1, p. 11833, dec. 2017, doi: 10.1038/s41598-017-11485-6.